White Rose Research Online

eprints@whiterose.ac.uk
https://eprints.whiterose.ac.uk
Universities of Leeds, Sheffield and York

Deposited via The University of Sheffield.

White Rose Research Online URL for this paper:
https://eprints.whiterose.ac.uk/id/eprint/218101/

Version: Published Version

Proceedings Paper:
Zanforlin, U., Lupo, C., Connolly, P.W.R. et al. (2023) Quantum super-resolution imaging and hypothesis testing. In: Figer, D.F. and Reimer, M., (eds.) Photonics for Quantum 2023. Photonics for Quantum 2023, 05-09 Jun 2023, Rochester, New York, United States. Proceedings of SPIE, 12633. Society of Photo-optical Instrumentation Engineers (SPIE). Article no: 1263308. ISSN: 0277-786X. EISSN: 1996-756X.

https://doi.org/10.1117/12.2671840

© 2023 Society of Photo Optical Instrumentation Engineers (SPIE). One print or electronic copy may be made for personal use only. Systematic reproduction and distribution, duplication of any material in this publication for a fee or for commercial purposes, or modification of the contents of the publication are prohibited.

Reuse
Items deposited in White Rose Research Online are protected by copyright, with all rights reserved unless indicated otherwise. They may be downloaded and/or printed for private study, or other acts as permitted by national copyright laws. The publisher or other rights holders may allow further reproduction and re-use of the full text version. This is indicated by the licence information on the White Rose Research Online record for the item.

Takedown
If you consider content in White Rose Research Online to be in breach of UK law, please notify us by emailing eprints@whiterose.ac.uk including the URL of the record and the reason for the withdrawal request.

UNIVERSITY OF LEEDS
University of Sheffield
UNIVERSITY of York

Quantum super-resolution imaging and hypothesis testing

Ugo Zanforlin[a], Cosmo Lupo[b], Peter W. R. Connolly[a], Pieter Kok[c], Gerald S. Buller[a], and Zixin Huang[d]

[a]School of Engineering and Physical Sciences, Heriot-Watt University, Edinburgh, United Kingdom
[b]Dipartimento Interateneo di Fisica, Politecnico di Bari, Italy
[c]Department of Physics and Astronomy, The University of Sheffield, Sheffield, United Kingdom
[d]School of Mathematical and Physical Sciences, Macquarie University, Sydney, Australia

ABSTRACT

Detecting the faint emission of a secondary source in the proximity of the much brighter one has been the most severe obstacle for using direct imaging in searching for exoplanets. Estimating the angular separation between two incoherent thermal sources is a also challenging task for direct imaging. Here, we experimentally demonstrate two tasks for super-resolution imaging based on hypothesis testing, quantum state discrimination and quantum imaging techniques. We show that one can significantly reduce the probability of error for detecting the presence of a weak secondary source (e.g. a planet), especially when the two sources have small angular separations. We reduce the experimental complexity down to a single two-input interferometer: we show that (1) this simple set-up is sufficient for the state discrimination task, and (2) if the two sources are of equal brightness, then this measurement can super-resolve their angular separation, saturating the quantum Cramér-Rao bound. By using a collection baseline of 5.3 mm, we resolve the angular separation of two sources that are placed 15 μm apart at a distance of 1.0 m with an accuracy of 1.7% – this is between 2 to 3 orders of magnitudes more accurate than shot-noise limited direct imaging.

Keywords: super-resolution, quantum imaging, quantum metrology

1. INTRODUCTION

Hypothesis testing, parameter estimation, and imaging are fundamental scientific tasks that can all be improved using quantum techniques.[1–3] A judicious choice of quantum probe state or measurement observable can significantly improve the information gained in a measurement. These improvements can manifest in a multitude of ways. For example, the noise in an image may be reduced,[4,5] or the resolution of the image may be improved beyond the classical Rayleigh limit.[6–9] Other improvements include ghost imaging, where information is extracted from quantum light that has not directly interacted with the object,[10,11] and quantum-enhanced non-linear microscopy.[12] Quantum lithography,[13,14] and quantum sensing[15–17] exploit entangled or correlated sources to enable precision beyond what is achievable classically. In microscopy, these techniques compete with classical super-resolution methods that use engineered sources that exhibit non-linear responses or exploit selective activation and bleaching of fluorophores.[18–21]

When source engineering is not an option, which is the case for astronomical observations, quantum techniques can beat the diffraction limit by unlocking all the information about amplitude and phase in the collected light. Traditionally, the resolution of an imaging system is limited by the the Rayleigh criterion:[7] the minimum angular separation that can be resolved is $\theta_{\min} \approx \lambda/D$, where λ is the wavelength and D is the diameter of the lens. A recent result for super-resolving a pair of incoherent sources has triggered much interest in the field.[3] It was shown that there is no loss of precision associated with estimating the sources' angular separation, even when their separation is smaller than $\theta_{\min}$.

Further author information: (Send correspondence to Z.H)
Z.H: E-mail: zixin.huang@mq.edu.au

Photonics for Quantum 2023, edited by Donald F. Figer, Michael Reimer,
Proc. of SPIE Vol. 12633, 1263308 · © 2023 SPIE · 0277-786X
doi: 10.1117/12.2671840

However, prior to measuring the separation, one needs to ensure that there are two sources and not just one. One straightforward method would be to use direct imaging (DI) to determine whether a secondary source is present. In a diffraction limited system, the image of a point-like object is not a point but has a finite spread characterised by the point-spread function (PSF). If the two sources overlap on the image screen, this blurring presents a severe practical obstacle to direct detection of exoplanets,[22,23] especially when one source is much dimmer than the other.

Quantum hypothesis testing techniques, on the other hand, can be used (Fig. 1) when the task is to determine whether a secondary source exists.[1] The goal is to minimise the probability of a false negative (missing the second source). If we are happy to accept a certain probability of false positives (type-I error), then the probability of a false negative (type-II error) is given by the quantum Stein Lemma.[24,25] This asymmetric error setting is particularly applicable to rare events such as exoplanet identification,[22,23] or events with important ramifications such as dimer detection in microscopy.[26] In quantum information theory, the two hypotheses – one source versus two sources – are modelled by two quantum states, ρ_0 and ρ_1. We consider n detection events, and work in the regime of highly attenuated signals where n corresponds to the number of photons received. We define α_n and β_n as the probabilities of type-I and type-II errors, respectively. Given a bounded probability of a type-I error, $\alpha_n < \delta$, the quantum Stein lemma[27,28] states that *

$$\beta_n = \exp\left[-nD(\rho_0||\rho_1) - \sqrt{nb}\,\Phi^{-1}(\delta) - O(\ln n)\right], \tag{1}$$

where

$$D(\rho_0||\rho_1) = \mathrm{Tr}\big[\rho_0(\ln\rho_0 - \ln\rho_1)\big], \tag{2}$$

is the quantum relative entropy (QRE),[29] $\Phi(\delta)$ is the Error Function, and b is the variance of the QRE.[30] In the limit of large n, the leading term in the error exponent is the one proportional to the QRE $D(\rho_0||\rho_1)$. Therefore $\beta_n \simeq \exp\left[-nD(\rho_0||\rho_1)\right]$ asymptotically. The quantum Stein lemma is already optimised over all possible measurements, therefore, it depends only on the two states to be discriminated, ρ_0 and ρ_1. The QRE provides a significant improvement in the error exponent β_n over the classical relative entropy for direct imaging,[1] thereby significantly reducing the probability of error, even when the two sources have small angular separations.

Once it is established with reasonable confidence that there are two sources, one can use quantum metrology to perform parameter estimation on the angular separation. The ultimate precision in the estimation is dictated by the quantum Cramér-Rao bound.[31] For any density matrix $\rho(\theta)$ with spectral decomposition $\rho(\theta) = \sum_i p_i\,|e_i\rangle\langle e_i|$ that encodes the information of the parameter θ, the mean square error $\Delta^2\theta$ is lower bounded by the quantum Fisher information (QFI) I_θ,

$$\Delta^2\theta \geq \frac{1}{nI_\theta}, \qquad I_\theta = 2\sum_{i,j}\frac{\langle e_i|\,\partial_\theta\rho\,|e_j\rangle}{p_i + p_j}, \tag{3}$$

where $\partial_\theta\rho = \partial\rho/\partial\theta$, and n is the number of photons detected. * The QFI represents the ultimate precision limit for the estimation of the given parameter, which may be achieved by some particular measurement. Obviously, not all measurements allow us to achieve it. For any given measurement, which yields a particular distribution of measurement outputs, the optimal mean square error is bounded by its associated classical Fisher information (FI), which is the classical counterpart of the QFI. Here we describe a method, based on interferometry, to experimentally achieve the ultimate quantum Cramér-Rao bound.[32] If a lens is used and the PSF is approximately Gaussian, this ultimate bound can be achieved by spatial-mode demultiplexing (SPADE) or similar methods.[3,33] For estimating the transverse separation between two equally bright sources, the QFI has been shown to be finite and independent of the separation.[3] This is in contrast with DI, which allows us to estimate the separation with limited precision that drops to zero when the separation is small compared to the width of the PSF.

Sub-Rayleigh super-resolution imaging through coherent detection of incoherent light is currently an active area of research.[5,34,35,35–47] However, implementing the optimal measurement is typically non-trivial. In this

*The quantum Stein Lemma and the quantum Cramér-Rao bound are usually defined in terms of number of copies of the state. However, here we work in the regime of highly attenuated signals and post-selected on photon detection events. Therefore, we refer to n as the number of photons detected. The two approaches differ only by a normalisation factor dictated by the overall transmission-detection efficiency.

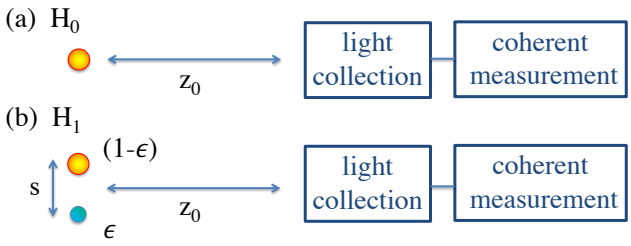

Figure 1. An optical imaging system is used to discern between two hypotheses, followed by parameter estimation. If hypothesis H_0 is true, only one source of intensity N is present; if H_1 is true, two sources are present, with total intensity N and the relative intensity is $\epsilon/(1-\epsilon)$. For H_1, angular separation between the two sources is $\theta = s/z_0$.

paper we achieve two goals: (1) we experimentally demonstrate clear sub-Rayleigh scaling for quantum state discrimination of singular versus binary sources, and (2) we approach the quantum Cramér-Rao bound for estimating the angular separation of two sources with equal brightness. Most importantly, we significantly simplify the required experimental complexity: the two goals are achieved with a single measurement set-up: all the above tasks can be performed with a simple interferometer with two spatial modes, i.e. we collect photons at two spatial locations. Then we perform photon counting at the output of the interferometer, and by analysing the statistics we can saturate both the QRE and the quantum Cramér-Rao bound.

2. RESULTS

2.1 The Model

First, consider the task of discriminating between one source or two sources with a separation s in the object plane. Hypothesis H_0 states that only one source is present, and it is positioned at x_0. Hypothesis H_1 states that two sources are present, where the first source is centred at x_0, and it has an angular separation $\theta = s/z_0$ with the second. Furthermore, they have relative intensities $(1-\epsilon)$ and ϵ respectively; without loss of generality, we assume $\epsilon \leq 0.5$. We will label a photon originating from the brighter source with intensity $(1-\epsilon)$ as $|\psi_{\text{star}}\rangle$, and the source with intensity ϵ as $|\psi_{\text{planet}}\rangle$. The two states on the image plane are generally non-orthogonal. The density matrices associated with the two hypotheses H_0 and H_1 are, respectively

$$\begin{aligned} \rho_0 &= |\psi_{\text{star}}\rangle\langle\psi_{\text{star}}| \ , \\ \rho_1 &= (1-\epsilon)\,|\psi_{\text{star}}\rangle\langle\psi_{\text{star}}| + \epsilon\,|\psi_{\text{planet}}\rangle\langle\psi_{\text{planet}}| \ . \end{aligned} \tag{4}$$

These two hypotheses can be discriminated by DI, in which case an optical system (which we may model as a thin converging lens) is used to create an image of the (unknown) source. The optical system is characterised by its PSF, which for a circular aperture is described by the Airy function. The latter, in turn, can be well-approximated by a Gaussian function with variance σ. In DI, the focused image is measured via pixel-by-pixel intensity detection, which in the weak-signal regime yields the empirical probability distribution of detecting a photon in each pixel. From the analysis of the data collected this way, one addresses the problem of hypothesis testing. The probability of a false negative is quantified by the classical analogue of the quantum Stein lemma, which expresses the error exponent in terms of the classical relative entropy (CRE), i.e. the Kullback-Leibler divergence. In the limit that $\theta \leq \sigma$ and $\epsilon \ll 1$ the classical relative entropy from DI is approximately $\left(\exp\left(\theta^2/\sigma^2\right) - 1\right)\epsilon^2/2$.[1] This quadratic scaling in ϵ formally expresses the challenges of using DI for exoplanet detection, especially when the planet is much dimmer and very close to the star.

By contrast, the QRE provides a $1/\epsilon$ improvement over the CRE.[1] An almost-optimal quantum measurement, SPADE,[3] is able to achieve linear scaling in ϵ by performing spatial Hermite-Gaussian mode sorting.[1] Though the SPADE device has recently been built and demonstrated,[48,49] the set-up is sensitive to misalignment of the sources' centroid,[3] cross-talk,[48] and is unsuitable for large-baseline instrument devices – SPADE is suited for circular lenses and mirrors and building such optical components larger than 10's of meters is infeasible. Here we present an alternative approach with reduced experimental complexity that can also be adapted for large-baselines devices.[50]

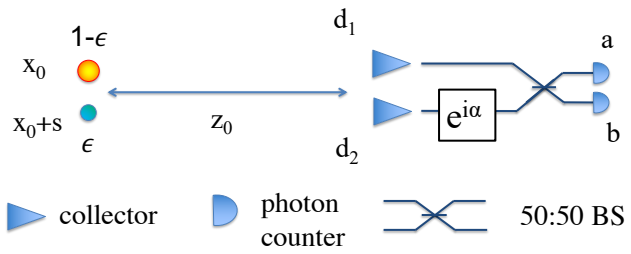

Figure 2. Schematic of two sources with a separation of s in the object plane, with relative intensities ϵ and $1-\epsilon$, at a distance z_0 from the collectors. Two collectors at d_1 and d_2 direct light into a two-input interferometer consisting of a phase shift of α and a 50:50 beam splitter, followed by photon counters. A collector can be any optical element that collects light. This could incorporate lenses or in the case of this experiment, two fibre connectors that present only the bare fibre core diameters in the direction of the source.

If instead of a lens we place two optical collectors, d_1 and d_2, separated by $d = |d_1 - d_2|$, and at a distance z_0 from the sources (see Fig. 2), then the states $|\psi_{\text{star}}\rangle$ and $|\psi_{\text{planet}}\rangle$ can be described as:

$$\begin{aligned} |\psi_{\text{star}}\rangle &= \frac{1}{\sqrt{2}}\Big(|d_1\rangle + e^{i\phi}\,|d_2\rangle \Big)\,, \\ |\psi_{\text{planet}}\rangle &= \frac{1}{\sqrt{2}}\Big(|d_1\rangle + e^{i\psi}\,|d_2\rangle \Big)\,, \end{aligned} \tag{5}$$

where ϕ, ψ are the optical path differences of the sources to the two collectors. In the paraxial regime, these are

$$\phi \approx \frac{kd\theta}{2}\,, \qquad \psi \approx \frac{-kd\theta}{2}\,, \tag{6}$$

where k is the wavenumber. Here we have assumed that the centre of the two collectors aligns with the centroid of the star-planet system for simplicity, but this is not necessary. In the limit of $\epsilon \ll 1$, the QRE between ρ_0 and ρ_1 is approximately[51]

$$D(\rho_0||\rho_1) \approx \frac{\theta^2 k^2 d^2 \epsilon}{4}\,. \tag{7}$$

Equation (7) is also linear in ϵ, thus has a factor $1/\epsilon$ improvement compared to the classical counterpart; an optimal measurement that saturates the QRE (i.e. the measurement's CRE that matches the QRE) is obtained by placing a phase shifter and a 50:50 BS after the two collectors, followed by photon counting. Given an imperfect interferometer with visibility ν, if there is no planet (H_0 is true), then the probabilities that the photon is detected at detectors a or b are

$$\begin{aligned} p_{H_0}(a) &= \frac{1}{2}\Big[1 + \nu\cos(\phi+\alpha)\Big]\,, \\ p_{H_0}(b) &= \frac{1}{2}\Big[1 - \nu\cos(\phi+\alpha)\Big]\,. \end{aligned} \tag{8}$$

where α is an adjustable phase. Otherwise, if H_1 is true, then the probabilities are

$$\begin{aligned} p_{H_1}(a) = \frac{1}{2}\Big[&(1-\epsilon)(1+\nu\cos(\phi+\alpha)) + \\ &\epsilon(1+\nu\cos(\psi+\alpha))\Big]\,, \\ p_{H_1}(b) = \frac{1}{2}\Big[&(1-\epsilon)(1-\nu\cos(\phi+\alpha)) + \\ &\epsilon(1-\nu\cos(\psi+\alpha))\Big]\,. \end{aligned} \tag{9}$$

Given that we know the output probabilities of the two hypotheses, the CRE of this measurement is given by the classical version of Eq. (2), where

$$D(p_{H_0}||p_{H_1}) = \sum_{i\in\{a,b\}} p_{H_0}(i)\big[\ln p_{H_0}(i) - \ln p_{H_1}(i)\big]\,. \tag{10}$$

The CRE is maximised for

$$\alpha \approx -kd\big[\epsilon(x_0+s)/z_0 + (1-\epsilon)(x_0)/z_0\big]\,, \tag{11}$$

and matches the QRE. Intuitively, this corresponds to the the point where $|p_{H_1}(a) - p_{H_0}(a)| = |p_{H_1}(b) - p_{H_0}(b)|$ is maximised.

We now move onto performing quantum parameter estimation on the state. When the source intensities are equal, the QFI for the above state is[32]

$$I_\theta = \frac{k^2 d^2}{4}, \tag{12}$$

which is constant in the effective pupil size d and independent of the angular separation θ. Hence, the angular separation can be estimated with constant precision even when its value is below the Rayleigh length, i.e. well beyond the diffraction limit. The very same measurement that achieves the maximum relative entropy, also allows to saturate the quantum Cramér-Rao bound dictated by the QFI (i.e. the measurement achieves the minimum uncertainty). Define $a^{\dagger'}_{d_1}(a^{\dagger'}_{d_2})$ to be the creation operator at the collector position d_1 (d_2). The adjustable phase shift α and the beam splitter transform the operator as

$$\begin{aligned} a^{\dagger'}_{d_1} &\to \frac{1}{\sqrt{2}}\left(a^\dagger_{d_1} + a^\dagger_{d_2}\right), \\ a^{\dagger'}_{d_2} &\to \frac{e^{i\alpha}}{\sqrt{2}}\left(a^\dagger_{d_1} - a^\dagger_{d_2}\right). \end{aligned} \tag{13}$$

Applying the transformation in Eq. (13) to the state $\rho = 1/2\,(|\psi_{\text{star}}\rangle\langle\psi_{\text{star}}| + |\psi_{\text{planet}}\rangle\langle\psi_{\text{planet}}|)$, the probabilities of detecting the photon at either detector are

$$\begin{aligned} p_a(\phi,\alpha,\nu) &= \frac{1}{2}\Big[1 + \nu\cos(\alpha)\cos(\phi)\Big], \\ p_b(\phi,\alpha,\nu) &= \frac{1}{2}\Big[1 - \nu\cos(\alpha)\cos(\phi)\Big]. \end{aligned} \tag{14}$$

Here ϕ is the same as in Eq. (6). Determining ϕ statistically will provide an estimation on the angular separation, explained in the next sections. The maximum classical relative entropy and Fisher information are achieved around the phase values $\alpha = 0$ or π. At these values, the CRE coincides with the QRE, and the Fisher information coincides with the QFI.[32]

2.2 Experimental set-up

The experimental set-up is depicted in Fig. 3. A fibre-coupled vertical cavity surface-emitting laser (VCSEL) with 848.2 nm central wavelength (0.11 nm FWHM) is operated in pulsed mode at a repetition rate of 1 MHz. This specific wavelength is chosen as it provides a good trade-off between single-photon detection efficiency ($\approx 40\%$) with commercially available thick-junction silicon single photon avalanche diodes (Si-SPADs) detectors and tolerable optical loss in silica fibres (≈ 2.2 dB/km).[52] The resulting coherent states are then coupled into two electro-optic modulators (EOMs) enabling phase and amplitude modulations of the individual coherent states. An external arbitrary waveform generator (AWG) electrically drives the two modulators by means of randomised modulation patterns so that the resulting optical states resemble a pseudo-thermal source,[53] required for the incoherent sources specified by the model and tested using a Hanbury Brown and Twiss interferometer. This modulation approach provides absolute control over each coherent state emitted by the source, including preserving the coherent state for use in interferometric measurements. In the results presented in this paper, we alternate the pseudo-thermal state with a coherent state that acts as a reference. The reference pulses provide

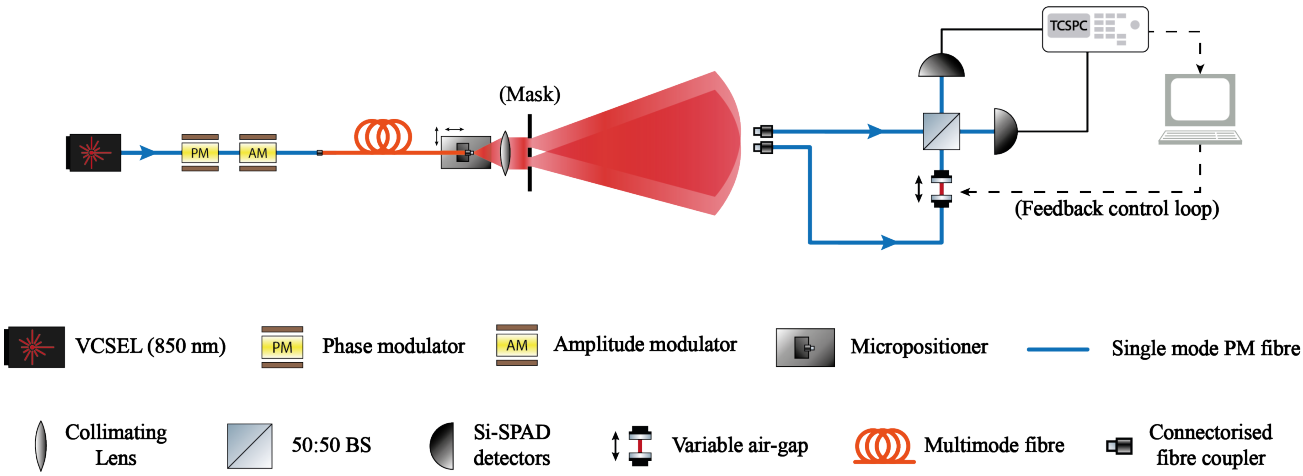

Figure 3. Experimental set-up. A VCSEL operated in pulsed mode generates coherent states that are phase and amplitude modulated to reproduce a pseudo thermal state. These states are then coupled into a multimode fibre and then collimated to a custom optical mask shaping the light beam into two pseudo-point-like sources. At 1 m distance, two single-mode polarisation-maintaining fibres collect the transmitted beam through connectorised couplers, followed by an adjustable air-gap that tunes the phase α, a 50:50 beam splitter and two single-photon detectors. These detectors are two Si-SPADs and register photon detection events storing their information onto a PC for post-processing via a TCSPC module. A feedback control system is used for interferometric stabilisation via the adjustable air gap.

the necessary interferometric stabilisation that is controlled via feedback from the two detectors, after the two pulses interfere at the beamsplitter. The alternate set of thermally modulated states instead are used to compute all relevant quantities detailed in our model.

After phase and amplitude modulation, the pseudo-thermal states are coupled into multimode optical fibres (8 m in length) in order to maximise mode dispersion and reduce wavefront spatial correlations due to the initial coupling of the VCSEL to single mode based optical components. The final thermal radiation is coupled into an adjustable aspheric collimator lens providing precise alignment with the remaining free-space optical components. Two pseudo-thermal sources are extracted from the collimated beam via a custom-made optical mask with two circular pinholes etched onto the surface, effectively reproducing two idealised point-like sources corresponding to the two distant stars of our model. Different etched patterns were fabricated using laser-written lithography in order to study a wide range of configurations with pinhole dimensions ranging from 10 to 50 μm in diameter and with spatial separation spanning from just 15 μm to almost 1 cm.

A neutral density filter is mounted on a separate movable micro-positioner block (not shown) placed in front of one of the two pinholes reducing the transmitted optical power through one of the pinholes. This configuration creates a controlled intensity imbalance between the two pseudo thermal sources effectively creating one bright source (a distant star) and one dimmer source (a distant exoplanet). At 1 m from the mask, two single-mode polarisation maintaining (PM) optical fibres, separated by 5.3 mm, are mounted on a micropositioner block (not shown) coupling the transmitted light beams into a balanced interferometer whose output modes are monitored by Si-SPAD detectors. The collectors used with the PM fibres are commercial fibre connectors with the bare fibre cores facing the approximate direction of the source. An adjustable air-gap is placed in one of the two optical paths allowing us to loss-balance the interferometer as well as providing direct control over the optical path-length difference. A time-correlated single photon counting (TCSPC) unit processes the generated timetags with 1 ps resolution enabling fast readout times as well as full digital post-processing. For each configuration of the set-up, 25 individual measurements are taken with a 5 s integration time in order to reduce Poissonian errors associated with photon-count data. An active feedback mechanism is implemented to ensure high interferometric visibility ($> 99\%$) during the entire duration of the data acquisition by means of a piezoelectric actuator adjusting the path-length difference of the interferometer via the air-gap (see Fig. 3).

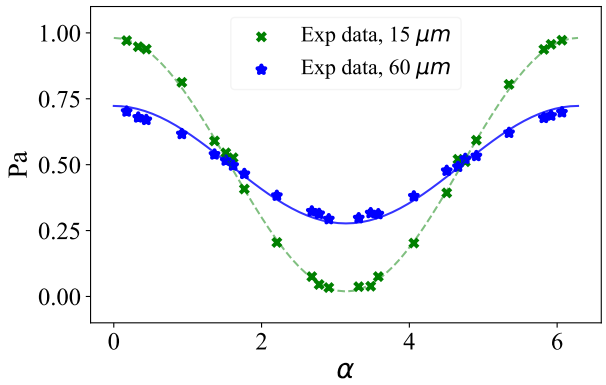

Figure 4. Photon detection probability of one of the detectors, as a function of the applied phase α, which is adjusted using the distance of the air-gap. The data shown are for $\epsilon = 0.5$, for physical separations of 1.5×10^{-5} m and 6.0×10^{-5} m; the angular separation are 1.48×10^{-5} rad and 5.9×10^{-5} rad respectively.

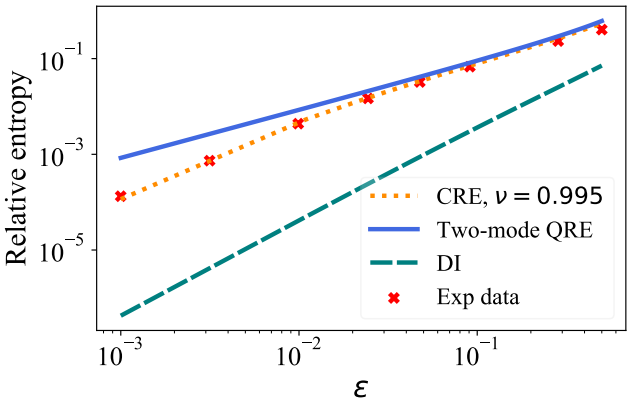

Figure 5. Relative entropy of the two hypothesis for different values of ϵ, using an angular separation of 5.9×10^{-5} rad. The plots shows: (1) the QRE of the two-mode state (blue solid line), (2) the CRE of the measurement maximised over α, given $\nu = 0.995$ (orange dotted line), (3) the CRE for shot-noise limited direct imaging (DI, teal dashed line), and (4) the experimental data points (red crosses).

2.3 Experimental Results

We experimentally measured the probability of the photon arriving at detectors a and b. As an example, in Fig. 4 we show the probability of the photon arriving at detector a for $\epsilon = 0.5$ and angular As expected, the contrast is higher for smaller separations: in the limit of small θ, the smaller the separation, the more spatially coherent the light becomes. In the limit that $\theta = 0$, we have a point source and the visibility should be 100% in theory.

First, we compute the relative entropies of the two scenarios. In Fig. 5 we present the CRE of the measurement for different values of ϵ using an angular separation of 5.9×10^{-5} rad. For comparison, we also show the relative entropy for direct imaging using a lens with a diameter equal to the fibre separation of 5.3 mm (assuming a Gaussian PSF). Fig. 5 shows the distinct difference in scaling in ϵ between our method and DI. For $\epsilon > 10^{-2}$, we see that the two-mode CRE matches the two-mode QRE well. Due to experimental imperfections, around $\epsilon \sim 10^{-3}$ the achievable relative entropy has significantly deviated from the ideal quantum case, but still surpasses the DI limit by two orders of magnitude.

We now present the method of analysis and results for estimating the angular separation. We use maximum likelihood estimation to first extract the optical path difference ϕ between the source and the two collectors, and then obtain an estimator for the angular separation θ. Our method for extracting ϕ is a simpler version of the

phase estimation method used in Refs.[54,55] We can determine ϕ directly from the detection statistics. To choose the estimator, it is useful to determine a probability density function for ϕ based on the detection results.

The probability density function for ϕ, $P(\phi)$, can be determined from Bayes' theorem as follows: prior to any detected photons, we assume no knowledge of ϕ, and the corresponding prior distribution is therefore $P_0(\phi) = 1/(2\pi)$. After one detection event $\mu = a, b$ and adjustable phase α, we have

$$P(\phi \,|\, \mu, \alpha, \nu) \propto \mathcal{P}(\mu \,|\, \phi, \alpha, \nu)\, P_0(\phi \,|\, \alpha, \nu). \tag{15}$$

where $\mathcal{P}(\mu \,|\, \phi, \alpha, \nu)$ is the update probability distribution. After m detection events, the vector of measurement outcomes is $\vec{\mu}_m = (\mu_1, \mu_2, \ldots, \mu_m)$, where each element $\mu_j \in \{a, b\}$, with $j \in [1, m]$, corresponds to the detector a or b that signalled the presence of the photon. The probability density function for ϕ is then[55]

$$P(\phi \,|\, \vec{\mu}_m, \alpha, \nu) \propto \mathcal{P}(\mu_m \,|\, \phi, \alpha, \nu)\, P(\phi \,|\, \vec{\mu}_{m-1}, \alpha, \nu)\,, \tag{16}$$

where the proportionality constant is determined by normalising the distribution.

In order to obtain an analytic form for $P(\phi \,|\, \vec{\mu}_m, \alpha, \nu)$, we express it as a Fourier series

$$P(\phi \,|\, \vec{\mu}_m, \alpha, \nu) = \frac{1}{2\pi} \sum_{k=-m}^{m} a_k e^{ik\phi}\,, \tag{17}$$

where a_k depends on $\vec{\mu}_m$, α and ν. After each detection event, we can write the updated distribution in this Fourier form as well. For example, if detector b fires, then following from Eq. (14),

$$\mathcal{P}(\mu = b \,|\, \phi, \alpha, \nu) = \frac{1}{2}\Big[1 - \nu \cos(\alpha) \cos(\phi)\Big]\,, \tag{18}$$

which we can rewrite as

$$\begin{aligned} \mathcal{P}(\mu = b \,|\, \phi, \alpha, \nu) = \frac{1}{2} - \frac{1}{4}\nu \cos(\alpha)\, e^{i\phi} - \\ \frac{1}{4}\nu \cos(\alpha)\, e^{-i\phi}\,. \end{aligned} \tag{19}$$

Therefore the update coefficients are $a_0 = \pi, a_1 = a_{-1} = -\frac{\pi}{2}\nu\cos(\alpha)$. The factor $\nu\cos(\alpha)$ is computed directly from the coherent state statistics . Before the first detection (the prior distribution), Eq. (17) contains only one term, $a_0 = 1$. After each detection event the number of Fourier coefficients grows by 2 (the $\pm m$ terms in the Fourier expansion). The coefficients a_k are updated using Eqs. (14) and (16).

As an example, Fig. 6 shows the probability density function $P(\phi)$, calculated based on Eq. (17) after 12740 detection events where 1478 were output at detector b, with $\nu\cos(\alpha) = 0.981$. Since $\cos(\phi)$ is an even function, there are two peaks, symmetrically placed around zero. We require only the magnitude of ϕ in the estimation of the angular separation θ.

Following maximum likelihood estimation, the value of ϕ at the maximum of $P(\phi)$ becomes our estimate, and the estimate of the separation θ is then given by

$$\hat{\theta}_{\text{est}} = 2|\phi|/(kd)\,. \tag{20}$$

Once this estimate is obtained, we use the mean-square error (MSE) to quantify the precision, given by

$$\text{MSE}(\theta) = \Delta^2\theta + (\bar{\theta} - \theta_{\text{true}})^2\,. \tag{21}$$

Here $\bar{\theta}$ is the mean value of the estimates, and θ_{true} is the true value of the angle, which in this case is accessible via direct measurement. The MSE is equal to the variance for unbiased measurements and appropriately penalises biased estimates as well.

For each value of the angular separation we obtained 25 different estimates, each detecting approximately $n \approx 60\,000$ photons. Figure 7 shows the MSE multiplied by $n \times I_\theta$. The experimental data points are indicated

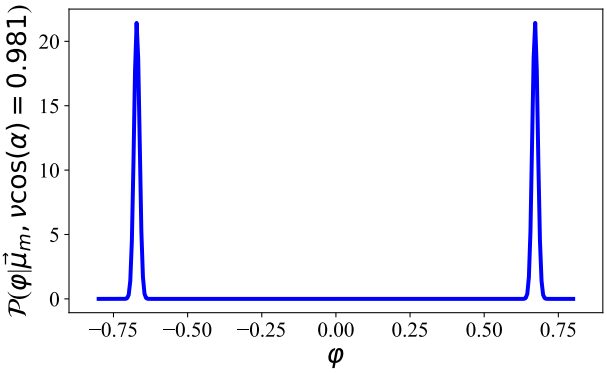

Figure 6. The probability density function for ϕ, after 12740 detection events of which 1478 were from detector b.

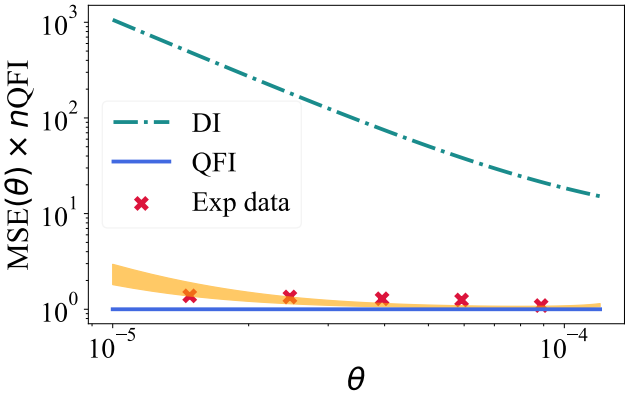

Figure 7. The mean squared error (MSE) of estimating the angular separation between two equally bright sources, normalised by the QFI, for different values of angular separation. The plot shows (1) the normalised QFI, which is equal to 1 here, and is constant across the whole range of angular separations θ (blue solid line); (2) the MSE for shot-noise limited DI (teal dotted-dashed line); (3) the Fisher information for an interferometer with a visibility-phase factor $\nu\cos(\alpha)$ between 0.965 and 0.985 (orange shaded region); (4) the experimentally achieved MSE (red crosses).

by red crosses, and the achievable precision for shot-noise limited DI (using a circular lens of diameter 5.3 mm) is indicated by the dash-dotted line.

Experimentally, the data was collected with the factor $\nu\cos(\alpha)$ between 0.96 and 0.985. This is the shaded orange region in Fig. 7. The quantum Cramér-Rao bound is equal to 1 in this figure (blue solid line). We obtained unbiased estimates for values of angular separation θ that dramatically beat the Rayleigh limit. When $\theta = 1.5 \times 10^{-6}$ rad, the root-mean-square errors are within 1.7% of the real value, which is two to three orders of magnitude more accurate than what is achievable with DI using a lens of the same diameter. For all the measured angular separations the MSE stayed within a factor 2 of the quantum Cramér-Rao bound.

3. DISCUSSION

In this work we have analysed theoretically, and demonstrated experimentally, two tasks for super-resolution imaging based on quantum state discrimination and quantum parameter estimation. Estimating the angular separation between two sources is a challenging task for direct imaging, especially when their angular separation is smaller than the point spread function of the imaging system. The task of determining whether there are one or two sources is in itself a difficult task, especially when one source is much dimmer than the other.

In this work, we solved both these problems and, compared with previous works,[1,33,56] we have reduced the experimental complexity down to a simple two-input interferometer: we show that a simple set-up achieves

sub-Rayleigh scaling for the state discrimination task, and if the two sources are of equal brightness, then this measurement can optimally estimate their angular separation, saturating the quantum Cramér-Rao bound.

We developed the theoretical analysis in the framework of single photons. However, the results extend to the regime of thermal sources as discussed in Ref.[1] The experiment was conducted with weak thermal sources, where the probability of detecting multiple photons is highly suppressed. This reflects the fact that the measurement is post-selecting on single-photon events, which explains why the experimental data saturates the single-photon quantum limit. A similar observation was made for the problem of estimating the transverse separation.[35] In the absence of background noise, losses do not affect our resolution apart from reducing the total photon count.

Our experiment also shows a practical optical set-up that could potentially be integrated with current stellar interferometers. However, this would require a different approach for the phase stabilisation of the interferometer. For example, the stabilisation could be provided by a ground-based coherent source or an artificial guide star which are suitably multiplexed into the interferometry system.

Our set-up is compatible with existing two-mode interferometers: the two-mode model assumes that the dimension of the collectors is much smaller compared to the spatial separation of the collectors d. For optical interferometers where the separation between arms is of the order of $\approx$ 100's m, collection using lenses and compound mirrors would be appropriate. For telescopes with point-spread functions that have 10's of milliarcseconds in resolution, we expect our method to be able to distinguish, or measure the separation of binary stars to precisions well-above direct imaging. As an example, the exoplanet LkCa 15 c[57] was observed with a Large Binocular Telescope (LBT) with a diffraction-limited PSF of $\approx$ 29 milliarcseconds (wavelength at 2.18 μm, 7 m in baseline). Using our method, if the instrument has visibility $\nu \geq 98\%$ (achieved by CHARA[58]), such an instrument can resolve two binary stars with separations less than 10 milliarcseconds.

In order to achieve the desired precision, we need a sufficient number of photon counts acquired over a time period during which the phase is stabilised. Naturally, the phase stabilisation will be highly dependent on the environment. One approach is that our system could be entirely translated into a planar waveguide architecture where light from a telescope could be collimated directly into laser-inscribed couplers greatly reducing optical losses and improving phase stabilisation due to the reduced dimensions of the interferometer.[59] Moreover, our system could improve the MSE of estimating even smaller angular separations by increasing the number of collected photons, but higher interferometric visibility levels ($\approx$ 99%) would be necessary to avoid signal degradation due to sub-optimal α values.

In our work we used pulsed light for both the reference signals and the pseudo thermal states. In a practical implementation, a celestial body would show a continuous form of radiation with a broad optical spectrum[60,61] which limits the interferometric visibility. However, our system can be easily adapted to implement narrow bandpass filters to select the right bandwidth for the detection stage at the cost of a reduced photon level. Moreover, Si-SPADs could be replaced with SNSPDs for faster sampling time, higher detection efficiencies and reduced dark counts and timing jitter.

Recently, there has been a renewed interest in two-photon interferometry (intensity interferometry).[62,63] Compared to those techniques, our method requires phase-stabilisation of the interferometer, but makes use of every photon received. The two-photon methods can achieve a very large baseline without needing an optical link between the system (or phase stabilisation), but suffer from low probability of successful detection events. In principle, if one has access to a quantum-enabled large baseline optical interferometer of the same baseline (such as those described in Ref.[64]), our scheme achieves much higher precision.

Here we have focused on the most simple scenario of discriminating one versus two point-like sources, using a two-mode interferometer. Future work could explore the hypothesis testing for discriminating between multiple sources of different brightness, composite hypothesis testing, and the number of modes the interferometer would require for such tasks.

ACKNOWLEDGMENTS

Z.H. is supported by a Sydney Quantum Academy Postdoctoral Fellowship. C.L. is supported by the EPSRC Quantum Communications Hub, Grant No. EP/T001011/1. This work is funded in part by the EPSRC

grant Large Baseline Quantum-Enhanced Imaging Networks, Grant No. EP/V021303/1. We thank Pieter Kok, Christian Schwab, Stefano Pirandola, and Martin Plenio for insightful feedback.

REFERENCES

[1] Huang, Z. and Lupo, C., "Quantum hypothesis testing for exoplanet detection," *Phys. Rev. Lett.* **127**, 130502 (Sep 2021).

[2] Giovannetti, V., Lloyd, S., and Maccone, L., "Quantum-enhanced measurements: beating the standard quantum limit," *Science* **306**(5700), 1330–1336 (2004).

[3] Tsang, M., Nair, R., and Lu, X.-M., "Quantum theory of superresolution for two incoherent optical point sources," *Phys. Rev. X* **6**, 031033 (Aug 2016).

[4] Brida, G., Genovese, M., and Berchera, I. R., "Experimental realization of sub-shot-noise quantum imaging," *Nature Photonics* **4**(4), 227 (2010).

[5] Howard, L. A., Gillett, G. G., Pearce, M. E., Abrahao, R. A., Weinhold, T. J., Kok, P., and White, A. G., "Optimal imaging of remote bodies using quantum detectors," *Phys. Rev. Lett.* **123**, 143604 (Sep 2019).

[6] Born, M. and Wolf, E., [*Principles of optics*], Elsevier (2013).

[7] Rayleigh, L., "Xxxi. investigations in optics, with special reference to the spectroscope," *The London, Edinburgh, and Dublin Philosophical Magazine and Journal of Science* **8**(49), 261–274 (1879).

[8] Giovannetti, V., Lloyd, S., Maccone, L., and Shapiro, J. H., "Sub-rayleigh-diffraction-bound quantum imaging," *Phys. Rev. A* **79**, 013827 (Jan 2009).

[9] Unternährer, M., Bessire, B., Gasparini, L., Perenzoni, M., and Stefanov, A., "Super-resolution quantum imaging at the heisenberg limit," *Optica* **5**(9), 1150–1154 (2018).

[10] Shapiro, J. H. and Boyd, R. W., "The physics of ghost imaging," *Quantum Information Processing* **11**(4), 949–993 (2012).

[11] Erkmen, B. I. and Shapiro, J. H., "Unified theory of ghost imaging with gaussian-state light," *Phys. Rev. A* **77**, 043809 (Apr 2008).

[12] Casacio, C. A., Madsen, L. S., Terrasson, A., Waleed, M., Barnscheidt, K., Hage, B., Taylor, M. A., and Bowen, W. P., "Quantum-enhanced nonlinear microscopy," *Nature* **594**(7862), 201–206 (2021).

[13] D'Angelo, M., Chekhova, M. V., and Shih, Y., "Two-photon diffraction and quantum lithography," *Phys. Rev. Lett.* **87**, 013602 (Jun 2001).

[14] Kok, P., Boto, A. N., Abrams, D. S., Williams, C. P., Braunstein, S. L., and Dowling, J. P., "Quantum-interferometric optical lithography: Towards arbitrary two-dimensional patterns," *Phys. Rev. A* **63**, 063407 (May 2001).

[15] Costa-Fernández, J. M., Pereiro, R., and Sanz-Medel, A., "The use of luminescent quantum dots for optical sensing," *TrAC Trends in Analytical Chemistry* **25**(3), 207–218 (2006).

[16] Degen, C. L., Reinhard, F., and Cappellaro, P., "Quantum sensing," *Rev. Mod. Phys.* **89**, 035002 (Jul 2017).

[17] Pirandola, S., Bardhan, B. R., Gehring, T., Weedbrook, C., and Lloyd, S., "Advances in photonic quantum sensing," *Nature Photonics* **12**, 724 (2018).

[18] Ram, S., Ward, E. S., and Ober, R. J., "Beyond rayleigh's criterion: a resolution measure with application to single-molecule microscopy," *Proceedings of the National Academy of Sciences* **103**(12), 4457–4462 (2006).

[19] Thorley, J. A., Pike, J., and Rappoport, J. Z., "Super-resolution microscopy: a comparison of commercially available options," in [*Fluorescence Microscopy*], 199–212, Elsevier (2014).

[20] Small, A. and Stahlheber, S., "Fluorophore localization algorithms for super-resolution microscopy," *Nature methods* **11**(3), 267 (2014).

[21] Mortensen, K. I., Churchman, L. S., Spudich, J. A., and Flyvbjerg, H., "Optimized localization analysis for single-molecule tracking and super-resolution microscopy," *Nature methods* **7**(5), 377 (2010).

[22] Wright, J. T. and Gaudi, B. S., "Exoplanet detection methods," *Planets, Stars and Stellar Systems: Volume 3: Solar and Stellar Planetary Systems* , 489–540 (2013).

[23] Fischer, D., Howard, A., Laughlin, G., Macintosh, B., Mahadevan, S., Sahlmann, J., and Yee, J., "Exoplanet detection techniques," *Protostars and Planets VI* , 715 (2014).

[24] Hiai, F. and Petz, D., "The proper formula for relative entropy and its asymptotics in quantum probability," *Commun. Math. Phys* **143**, 99–114 (1991).

[25] Ogawa, T. and Nagaoka, H., "Strong converse and stein's lemma in quantum hypothesis testing," *IEEE Trans. Inf. Th.* **46**, 2428–2433 (2000).

[26] Nan, X., Collisson, E. A., Lewis, S., Huang, J., Tamgüney, T. M., Liphardt, J. T., McCormick, F., Gray, J. W., and Chu, S., "Single-molecule superresolution imaging allows quantitative analysis of raf multimer formation and signaling," *Proceedings of the National Academy of Sciences* **110**(46), 18519–18524 (2013).

[27] Li, K. et al., "Second-order asymptotics for quantum hypothesis testing," *Annals of Statistics* **42**, 171 (2014).

[28] Tomamichel, M. and Hayashi, M., "A hierarchy of information quantities for finite block length analysis of quantum tasks," *IEEE Transactions on Information Theory* **59**(11), 7693–7710 (2013).

[29] Wilde, M. M., [*Quantum information theory*], Cambridge University Press (2013).

[30] Wilde, M. M., Tomamichel, M., Lloyd, S., and Berta, M., "Gaussian hypothesis testing and quantum illumination," *Phys. Rev. Lett.* **119**, 120501 (Sep 2017).

[31] Paris, M. G., "Quantum estimation for quantum technology," *International Journal of Quantum Information* **7**(supp01), 125–137 (2009).

[32] Lupo, C., Huang, Z., and Kok, P., "Quantum limits to incoherent imaging are achieved by linear interferometry," *Phys. Rev. Lett.* **124**, 080503 (Feb 2020).

[33] Tsang, M., "Resolving starlight: a quantum perspective," *Contemporary Physics* **60**(4), 279–298 (2019).

[34] Lupo, C. and Pirandola, S., "Ultimate precision bound of quantum and subwavelength imaging," *Phys. Rev. Lett.* **117**, 190802 (Nov 2016).

[35] Nair, R. and Tsang, M., "Far-field superresolution of thermal electromagnetic sources at the quantum limit," *Phys. Rev. Lett.* **117**, 190801 (Nov 2016).

[36] Backlund, M. P., Shechtman, Y., and Walsworth, R. L., "Fundamental precision bounds for three-dimensional optical localization microscopy with poisson statistics," *Phys. Rev. Lett.* **121**, 023904 (Jul 2018).

[37] Yu, Z. and Prasad, S., "Quantum limited superresolution of an incoherent source pair in three dimensions," *Phys. Rev. Lett.* **121**, 180504 (Oct 2018).

[38] Napoli, C., Piano, S., Leach, R., Adesso, G., and Tufarelli, T., "Towards superresolution surface metrology: Quantum estimation of angular and axial separations," *Phys. Rev. Lett.* **122**, 140505 (Apr 2019).

[39] Pirandola, S., Laurenza, R., Lupo, C., and Pereira, J. L., "Fundamental limits to quantum channel discrimination," *npj Quantum Information* **5**, 50 (2019).

[40] Dutton, Z., Kerviche, R., Ashok, A., and Guha, S., "Attaining the quantum limit of superresolution in imaging an object's length via predetection spatial-mode sorting," *Phys. Rev. A* **99**, 033847 (Mar 2019).

[41] Paúr, M., Stoklasa, B., Hradil, Z., Sánchez-Soto, L. L., and Rehacek, J., "Achieving the ultimate optical resolution," *Optica* **3**(10), 1144–1147 (2016).

[42] Tham, W.-K., Ferretti, H., and Steinberg, A. M., "Beating rayleigh's curse by imaging using phase information," *Phys. Rev. Lett.* **118**, 070801 (Feb 2017).

[43] Donohue, J. M., Ansari, V., Řeháček, J., Hradil, Z., Stoklasa, B., Paúr, M., Sánchez-Soto, L. L., and Silberhorn, C., "Quantum-limited time-frequency estimation through mode-selective photon measurement," *Phys. Rev. Lett.* **121**, 090501 (Aug 2018).

[44] Parniak, M., Borówka, S., Boroszko, K., Wasilewski, W., Banaszek, K., and Demkowicz-Dobrzański, R., "Beating the rayleigh limit using two-photon interference," *Phys. Rev. Lett.* **121**, 250503 (Dec 2018).

[45] Paúr, M., Stoklasa, B., Grover, J., Krzic, A., Sánchez-Soto, L. L., Hradil, Z., and Řeháček, J., "Tempering rayleigh's curse with psf shaping," *Optica* **5**(10), 1177–1180 (2018).

[46] Hassett, J., Malhorta, T., Alonso, M., Boyd, R., Rafsanjani, S. H., and Vamivakas, A., "Sub-rayleigh limit localization with a spatial mode analyzer," in [*Laser Science*], JW4A–124, Optical Society of America (2018).

[47] Zhou, Y., Yang, J., Hassett, J. D., Rafsanjani, S. M. H., Mirhosseini, M., Vamivakas, A. N., Jordan, A. N., Shi, Z., and Boyd, R. W., "Quantum-limited estimation of the axial separation of two incoherent point sources," *Optica* **6**(5), 534–541 (2019).

[48] Boucher, P., Fabre, C., Labroille, G., and Treps, N., "Spatial optical mode demultiplexing as a practical tool for optimal transverse distance estimation," *Optica* **7**(11), 1621–1626 (2020).

[49] Fontaine, N. K., Ryf, R., Chen, H., Neilson, D. T., Kim, K., and Carpenter, J., "Laguerre-gaussian mode sorter," *Nature communications* **10**(1), 1–7 (2019).

[50] ten Brummelaar, T. A., McAlister, H. A., Ridgway, S. T., Bagnuolo Jr., W. G., Turner, N. H., Sturmann, L., Sturmann, J., Berger, D. H., Ogden, C. E., Cadman, R., Hartkopf, W. I., Hopper, C. H., and Shure, M. A., "First results from the CHARA array. II. A description of the instrument," *The Astrophysical Journal* **628**, 453–465 (Jul 2005).

[51] Zanforlin, U., Lupo, C., Connolly, P. W., Kok, P., Buller, G. S., and Huang, Z., "Optical quantum super-resolution imaging and hypothesis testing," *Nature Communications* **13**(1), 5373 (2022).

[52] Buller, G. S. and Collins, R. J., "Single-photon generation and detection," *Measurement Science and Technology* **21**, 012002 (nov 2009).

[53] Tatsi, G., Canning, D. W., Zanforlin, U., Mazzarella, L., Jeffers, J., and Buller, G. S., "Manipulating thermal light via displaced-photon subtraction," *Phys. Rev. A* **105**, 053701 (May 2022).

[54] Berry, D. W. and Wiseman, H. M., "Optimal states and almost optimal adaptive measurements for quantum interferometry," *Phys. Rev. Lett.* **85**, 5098–5101 (Dec 2000).

[55] Huang, Z., Motes, K. R., Anisimov, P. M., Dowling, J. P., and Berry, D. W., "Adaptive phase estimation with two-mode squeezed vacuum and parity measurement," *Phys. Rev. A* **95**, 053837 (May 2017).

[56] Grace, M. R. and Guha, S., "Quantum-optimal object discrimination in sub-diffraction incoherent imaging," *arXiv:2107.00673* (2021).

[57] Sallum, S., Follette, K., Eisner, J. A., Close, L. M., Hinz, P., Kratter, K., Males, J., Skemer, A., Macintosh, B., Tuthill, P., et al., "Accreting protoplanets in the lkca 15 transition disk," *Nature* **527**(7578), 342–344 (2015).

[58] Anugu, N., Le Bouquin, J.-B., Monnier, J. D., Kraus, S., Setterholm, B. R., Labdon, A., Davies, C. L., Lanthermann, C., Gardner, T., Ennis, J., et al., "Mirc-x: a highly sensitive six-telescope interferometric imager at the chara array," *The Astronomical Journal* **160**(4), 158 (2020).

[59] Canning, D. W., Donaldson, R. J., Mukherjee, S., Collins, R. J., Mazzarella, L., Zanforlin, U., Jeffers, J., Thomson, R. R., and Buller, G. S., "On-chip implementation of the probabilistic quantum optical state comparison amplifier," *Optics Express* **27**, 31713 (oct 2019).

[60] Klochkova, V. G., Chentsov, E. L., Tavolganskaya, N. S., and Shapovalov, M. V., "Optical spectrum of the post-agb star hd56126 in the wavelength interval 4010-8790 å å," *Astrophysical Bulletin* **62**, 162–192 (Jun 2007).

[61] Maryeva, O. and Abolmasov, P., "Modelling the optical spectrum of Romano's star," *Monthly Notices of the Royal Astronomical Society* **419**, 1455–1464 (12 2011).

[62] Stankus, P., Nomerotski, A., Slosar, A., and Vintskevich, S., "Two-photon amplitude interferometry for precision astrometry," *arXiv:2010.09100* (2020).

[63] Bojer, M., Huang, Z., Karl, S., Richter, S., Kok, P., and Von Zanthier, J., "A quantitative comparison of amplitude versus intensity interferometry for astronomy," *New Journal of Physics* **24**(4), 043026 (2022).

[64] Khabiboulline, E. T., Borregaard, J., De Greve, K., and Lukin, M. D., "Optical interferometry with quantum networks," *Phys. Rev. Lett.* **123**, 070504 (Aug 2019).